

Adversarial Body Shape Search for Legged Robots

Takaaki Azakami

Graduate School of Science and Engineering
Chiba University

Chiba, Japan

Email: takaaki.azakami@chiba-u.jp

Hiroshi Kera

Graduate School of Engineering
Chiba University

Chiba, Japan

Email: kera@chiba-u.jp

Kazuhiko Kawamoto

Graduate School of Engineering
Chiba University

Chiba, Japan

Email: kawa@faculty.chiba-u.jp

Abstract—We propose an evolutionary computation method for an adversarial attack on the length and thickness of parts of legged robots by deep reinforcement learning. This attack changes the robot body shape and interferes with walking—we call the attacked body as *adversarial body shape*. The evolutionary computation method searches adversarial body shape by minimizing the expected cumulative reward earned through walking simulation. To evaluate the effectiveness of the proposed method, we perform experiments with three legged robots, Walker2d, Ant-v2, and Humanoid-v2 in OpenAI Gym. The experimental results reveal that Walker2d and Ant-v2 are more vulnerable to the attack on the length than the thickness of the body parts, whereas Humanoid-v2 is vulnerable to the attack on both of the length and thickness. We further identify that the adversarial body shapes break left-right symmetry or shift the center of gravity of the legged robots. Finding adversarial body shape can be used to proactively diagnose the vulnerability of legged robot walking.

Index Terms—Adversarial attack, Deep reinforcement learning, Legged robot control

I. INTRODUCTION

Deep reinforcement learning in robotics has been widely studied [1]; the vulnerability and robustness have also been attracting attention. In particular, the vulnerability to adversarial attacks is inherent to deep reinforcement learning, and improving the robustness is a considerable challenge [2], [3]. Among the adversarial attacks in robotics, the attack on state observations is a main topic, because they directly affect the control of robots.

In this study, we consider the adversarial attack on the body shape of legged robots, which is seen as an attack on environments, not the state observation. The attack adds adversarial perturbations to the length and thickness of the legged robots; we call the attacked body shape as *adversarial body shape*. Figure 1 illustrates the adversarial body shape search, where the adversarial attack makes the length of the bipedal robot’s leg shorter and throws the robot off balance. Robot body shape changes can occur owing to various factors such as oxidation of the metal material, adhesion of foreign matter to the surface, and formation of defects and dents caused by collision. If such changes are too small to detect, vulnerability is a potential risk. The adversarial attack can search small perturbations that causes walking instability of the legged robots. Thus, the adversarial body shape search can be used to proactively diagnose the vulnerability of robot walking.

This work was supported by JSPS KAKENHI Grant Numbers JP19K12039 and JP22H03658.

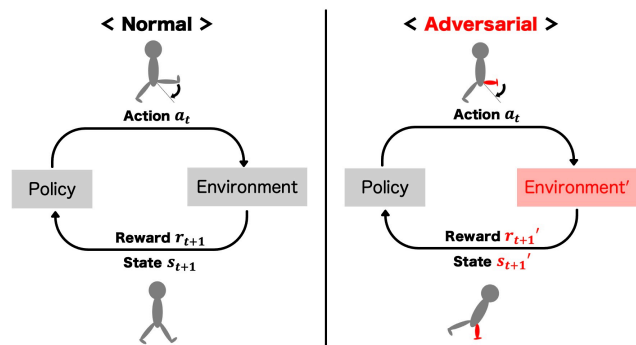
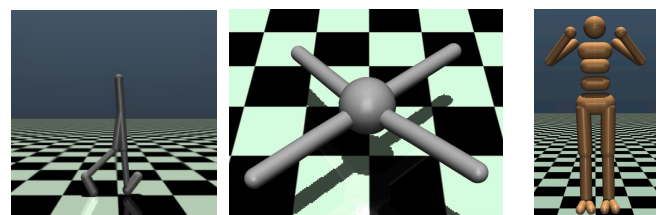


Fig. 1: Adversarial body shape search



(a) Walker2d-v2

(b) Ant-v2

(c) Humanoid-v2

Fig. 2: Legged robots

We propose a differential evolution method [4] for searching adversarial body shapes of the legged robots. The proposed search method is designed to reduce the cumulative reward earned by walking simulation of the legged robots. The rewards can be obtained only through walking simulation. Therefore, we employ evolutionary computation with walking simulation on a physical engine to search adversarial body shapes. We perform experiments with three legged robots: the bipedal robot Walker2d-v2, the quadruped robot Ant-v2, and the bipedal robot Humanoid-v2 [5], as shown in Fig. 2. These robot environments run on the physical engine MuJoCo [6]. We evaluate the effectiveness of the proposed search method in terms of the average cumulative rewards for 1000 walking simulations. The experimental results reveal that Walker2d and Ant-v2 are more vulnerable to the attack on the length than the thickness of the body parts, whereas, Humanoid-v2 is vulnerable to the attack on both of the length and thickness. In addition, we investigate the adversarial perturbations that interfere with the walking task for each body part and discover that the perturbations break left-right

symmetry or shift the center of gravity of the legged robots.

The main contributions of this study are as follows:

- We propose an evolutionary computation method with physical walking simulations for searching adversarial body shapes of legged robots. This method will be used to proactively diagnose the vulnerability of the legged robots.
- We discover the adversarial body shapes that interfere with the walking task for the first time.

II. RELATED WORK

Robot design optimization for legged robots has been studied. Several studies [7]–[9] jointly optimize robot design and reinforcement learning. Using REINFORCEMENT, Ha et al. [7] improve policies in environments such as BipedalWalker-2d and Ant-v1, and design more task-appropriate bodies. Schaff et al. [8] retain the distribution on the length and thickness of the legged robots: Hopper, Walker2d, and Ant. They use reinforcement learning to optimize the control policy by maximizing the expected reward for the design distribution. Luck et al. [9] combine design optimization and reinforcement learning to minimize the number of prototypes for optimal robot foot design, improving data efficiency. These studies optimize the robot design by maximizing the rewards. However, they do not consider the vulnerability inherent to the legged robots trained by reinforcement learning. Wang et al. [10] use evolutionary computation to design an optimal size and position of fish fins. To design that, neural graph evolution [11] is used, and the method iteratively evolves the graph structure using mutations. Desai et al. [12] propose an interactive computational design system that enables users to design legged robots with desired morphologies and behaviors. The interactive system automatically suggests candidate robot designs to achieve a specified behavior or task performance by an optimization algorithm. Although these studies do not use reinforcement learning, they still do not consider the vulnerability of the legged robots. In this study, we propose a method for detecting the vulnerability inherent to the body shapes of the legged robots trained by deep reinforcement learning.

III. ADVERSARIAL BODY SHAPE SEARCH

This section describes the adversarial body shape perturbation and the adversarial body shape generation algorithm.

A. Adversarial Body Shape Perturbation

We denote \mathbf{b} as a body shape vector consisting of the length or thickness of the body parts of legged robots in Fig. 2. We assume that body shape \mathbf{b} is constant over time. Body shape \mathbf{b} affects reward r_t through reward function $r(\cdot)$, i.e.,

$$r_t = r(\mathbf{s}_t, \mathbf{a}_t, \mathbf{b}) \quad (1)$$

where, \mathbf{a}_t is the action vector of a legged robot at time t , and reward r_t is computed by running a physical simulation for robot walking.

In this study, we perturb body shape \mathbf{b} as

$$\mathbf{b}_{\text{adv}} = \mathbf{b} + \delta \odot \mathbf{b} \quad (2)$$

Algorithm 1 Adversarial Body Shape Generation Algorithm

Require: Population size NP

- 1: Generate initial population of body shape perturbations $\{\delta_0^{(1)}, \dots, \delta_0^{(NP)}\}$ with $\delta_{j,0}^{(i)} \sim U([- \epsilon, \epsilon])$
 - 2: $G_{\min} \leftarrow \infty$
 - 3: **for** each generation $g = 1, 2, \dots$ **do**
 - 4: **for** each individual $i = 1, 2, \dots, NP$ **do**
 - 5: Compute adversarial shape $\mathbf{b}_{\text{adv}}^{(i)} = \mathbf{b} + \delta_{g-1}^{(i)} \odot \mathbf{b}$
 - 6: Generate trial individual $\mathbf{u}_g^{(i)}$ by mutation and crossover in Eqs. (7) and (8)
 - 7: Compute trial shape $\mathbf{b}_{\text{trial}}^{(i)} = \mathbf{b} + \mathbf{u}_g^{(i)} \odot \mathbf{b}$
 - 8: Compute average cumulative rewards in Eq. (6) for trial $\bar{G}(\mathbf{b}_{\text{trial}}^{(i)})$ and target $\bar{G}(\mathbf{b}_{\text{adv}}^{(i)})$
 - 9: **if** $\bar{G}(\mathbf{b}_{\text{trial}}^{(i)}) \leq \bar{G}(\mathbf{b}_{\text{adv}}^{(i)})$ **then**
 - 10: Accept trial individual $\delta_g^{(i)} \leftarrow \mathbf{u}_g^{(i)}$
 - 11: **if** $\bar{G}(\mathbf{b}_{\text{trial}}^{(i)}) < G_{\min}$ **then**
 - 12: $G_{\min} \leftarrow \bar{G}(\mathbf{b}_{\text{trial}}^{(i)})$
 - 13: Update best individual $\delta_{\text{best}} \leftarrow \delta_g^{(i)}$
 - 14: **end if**
 - 15: **else**
 - 16: Retain target individual $\delta_g^{(i)} \leftarrow \delta_{g-1}^{(i)}$
 - 17: **end if**
 - 18: **end for**
 - 19: **end for**
 - 20: **return** δ_{best}
-

where δ is an adversarial perturbation of body shape \mathbf{b} , and \odot is the Hadamard product. Equation (2) perturbs the ratio of the length or thickness of the parts of legged robots. For example, the length of the i -th body part, denoted by b_i , is perturbed by

$$b_{i,\text{adv}} = b_i + \delta_i b_i = (1 + \delta_i) b_i \quad (3)$$

Adversarial perturbation δ is computed by minimizing the expected cumulative reward as

$$\delta_{\text{best}} = \underset{\delta}{\operatorname{argmin}} E[G(\mathbf{b}_{\text{adv}})], \text{ subject to } \|\delta\|_{\infty} \leq \epsilon \quad (4)$$

where $\|\cdot\|_{\infty}$ indicates the maximum norm, ϵ is a small positive constant, and $G(\mathbf{b}_{\text{adv}})$ is the cumulative reward attacked by adversarial perturbation δ and is defined as

$$G(\mathbf{b}_{\text{adv}}) = \sum_{t=0}^{T-1} r(\mathbf{s}_t, \mathbf{a}_t, \mathbf{b}_{\text{adv}}). \quad (5)$$

The expectation in Eq. (4) is taken with respect to a trajectory of states and actions $\{s_0, a_0, s_1, a_1, \dots, s_{T-1}, a_{T-1}\}$, and the expected cumulative reward can be empirically estimated by running M waking simulations as

$$E[G(\mathbf{b}_{\text{adv}})] \approx \bar{G}(\mathbf{b}_{\text{adv}}) = \frac{1}{M} \sum_{m=1}^M G^{(m)}(\mathbf{b}_{\text{adv}}), \quad (6)$$

where $G^{(m)}(\mathbf{b}_{\text{adv}})$ is the reward obtained by the m -th walking simulation. In experiments, we set $M = 50$.

B. Evolutionary computation for Adversarial Body Shape

We employ a differential evolution method [4] to find the best perturbation δ_{best} in Eq. (4). Note that it is difficult to

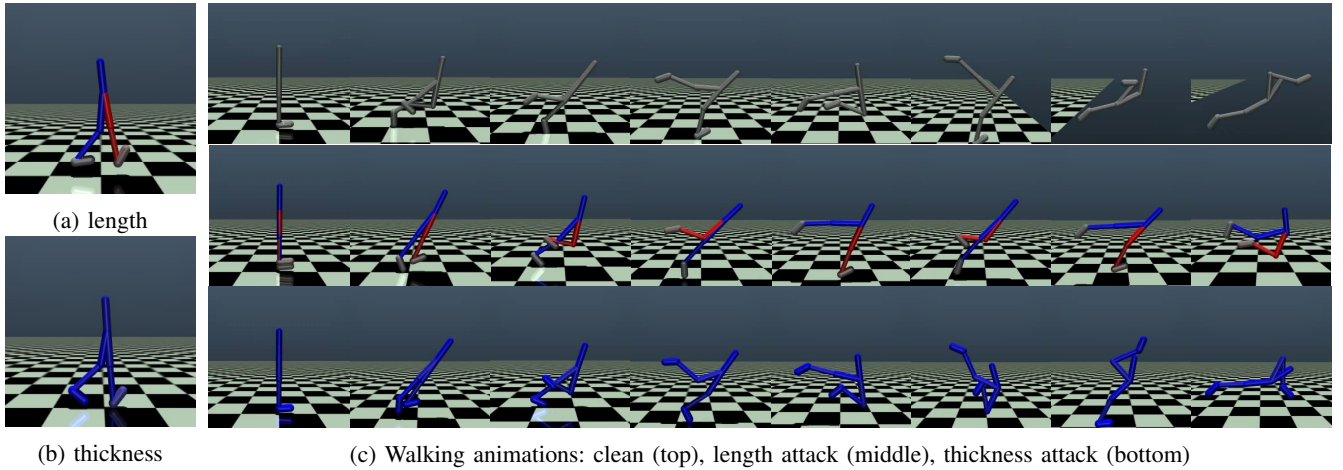


Fig. 3: Adversarial body shapes with length and thickness perturbations for Walker2d-v2.

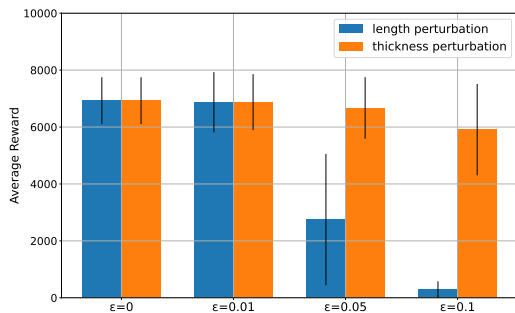


Fig. 4: Averages of the average cumulative rewards with attack strength $\epsilon = 0.0, 0.01, 0.05, 0.1$ for Walker2d-2d

compute the gradient of the cumulative reward, $G(\mathbf{b})$, with respect to \mathbf{b} because the computation of $G(\mathbf{b})$ requires physical simulations. Therefore, we cannot use efficient methods such as gradient descent. Our simulation-based adversarial attack is a black box attack [3].

We show the differential evolution method for adversarial body shape attack in **Algorithm 1**. For differential evolution, we first generate an initial population of body shape perturbations $\{\delta_0^{(1)}, \dots, \delta_0^{(NP)}\}$, where NP is the population size. Each element of initial individual $\delta_0^{(i)}$ is generated according to uniform distribution $U([- \epsilon, \epsilon])$. In differential evolution, the mutation and crossover of the population are performed. Mutant individual $\mathbf{v}_{g+1}^{(i)}$ at the $g+1$ -th generation is generated according to

$$\mathbf{v}_{g+1}^{(i)} = \delta_{\text{best}} + F(\delta_g^{(r_1)} - \delta_g^{(r_2)}), \quad (7)$$

where F is the parameter that adjusts the rate of mutation, and r_1, r_2 are randomly selected from the individual index set, $\{1, \dots, NP\}$. The best individual δ_{best} in Eq. (7) is the intermediate best until the g -th generation. The trial individual by crossover $\mathbf{u}_{g+1}^{(i)}$ is generated according to

$$\mathbf{u}_{j,g+1}^{(i)} = \begin{cases} \mathbf{v}_{j,g+1}^{(i)} & \text{if } r \leq CR \text{ or } j = j_r \\ \delta_{j,g}^{(i)} & \text{otherwise} \end{cases} \quad (8)$$

TABLE I: Adversarial body shape perturbation for thickness and length of Walker2d-v2

body part	length (%)	thickness (%)
torso	+4.73	+3.93
right thigh	+4.82	+4.91
right leg	+4.59	+4.19
right foot	+0.08	+4.62
left thigh	-4.74	+4.15
left leg	-3.80	+4.54
left foot	-0.36	+2.08

where subscript j indicates the j -th element of the vector, r is a uniform random number in $[0, 1]$, $CR = 0.7$ is a crossover constant, and j_r is a random element index.

IV. EXPERIMENT

To demonstrate the performance of the adversarial body shape search in **Algorithm 1**, we conducted experiments on a physical simulation environment MuJoCo [6] with three legged robots in OpenAI Gym [5]: Walker2d-v2, Ant-v2, and Humanoid-v2, as shown in Fig. 2.

A. Experimental setup

Before the experiments, we first trained these three robots until they can walk well using the proximal policy optimization (PPO) [13]. The PPO is a policy gradient-based reinforcement learning algorithm and suitable for continuous control. We set hyperparameters for training as follows: learning rate is $3.0 \cdot 10^{-5}$, epochs are 10, clip range is 0.1, batch size is 256, horizon is 2048. We designed reward functions to ensure that the robots do not fall and walk along the x -axis as fast as possible. The respective reward functions for Walker2d-v2, Ant-v2, and Humanoid-v2 are given as follows:

$$r_t = v_{fwd} - 10^{-3} \|\mathbf{u}\|^2 + 1.0, \quad (9)$$

$$r_t = v_{fwd} - 0.5 \|\mathbf{u}\|^2 - 0.5 \cdot 10^{-3} \|\mathbf{f}\|^2 + 1.0, \quad (10)$$

$$r_t = 5.0 v_{fwd} - 0.1 \|\mathbf{u}\|^2 - 0.5 \cdot 10^{-6} \|\mathbf{f}\|^2 + 4.0, \quad (11)$$

where v_{fwd} is the forward velocity, \mathbf{u} is the vector of joint torques, and \mathbf{f} is the impact force vector.

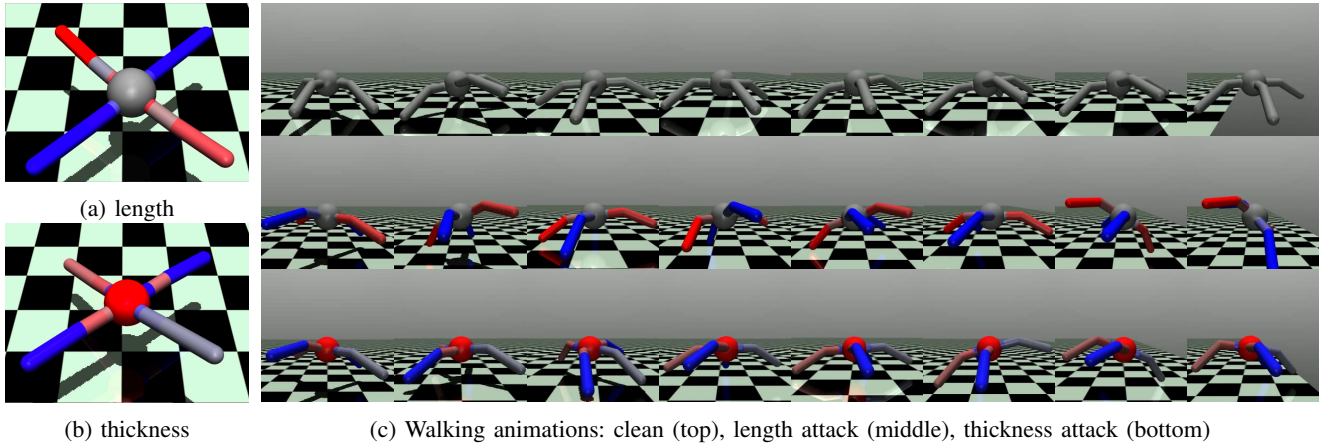


Fig. 5: Adversarial body shapes with length and thickness perturbations for Ant-v2.

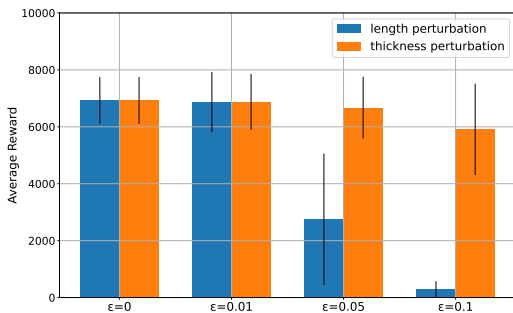


Fig. 6: Averages of the average cumulative rewards with attack strength $\epsilon = 0.0, 0.01, 0.05, 0.1$ for Ant-2d

For performance evaluation, we compute average cumulative rewards $\bar{C}(\mathbf{b}_{\text{adv}})$ in Eq. (6) 1000 times and then average them as

$$\frac{1}{1000} \sum_{i=1}^{1000} \bar{C}^{(i)}(\mathbf{b}_{\text{adv}}), \quad (12)$$

where $\bar{C}^{(i)}(\mathbf{b}_{\text{adv}})$ is the average cumulative reward at the i -th simulation run. Note that $\bar{C}(\mathbf{b}_{\text{adv}})$ can vary with each simulation run even if \mathbf{b}_{adv} is fixed, because action \mathbf{a}_t is stochastically generated according to policy network $\pi(\mathbf{a}_t | \mathbf{s}_t)$. To compute $\bar{C}(\mathbf{b}_{\text{adv}})$, we set the attack strength as $\epsilon = 0.0, 0.01, 0.05, 0.1$, where $\epsilon = 0.0$ means no attack. Following the literature on adversarial attack, we call the body shape with $\epsilon = 0.0$ the *clean* body, and use it as the baseline in this study. In differential evolution, we set the number of individuals to $NP = 14, 26, 38$ for Walker2d-v2, Ant-v2, and Humanoid-v2, respectively, and set the number of the generations to 100 for all the robots.

B. Adversarial body shape search

We investigated the performance evaluation for each legged robots: Walker2d-v2, Ant-v2, and Humanoid-v2.

1) *Walker2d-v2*: Figure 3 visualizes the perturbations of the length and thickness with $\epsilon = 0.05$. The blue body parts represent those that are longer or thicker than the clean ones, i.e., positive perturbations are added, while the red ones are

TABLE II: Adversarial body shape perturbation for thickness and length of Ant-v2

body part	length (%)	thickness(%)
torso	-	-4.51
left front thigh	-1.88	+2.95
left front leg	+0.30	-1.83
left front foot	-4.68	-1.28
right front thigh	+3.13	+4.29
right front leg	+4.70	-1.41
right front foot	+4.85	+4.38
left back thigh	+2.05	-1.06
left back leg	+4.17	-1.76
left back foot	+4.90	+4.12
right back thigh	-2.67	+1.94
right back leg	-0.54	+0.67
right back foot	-2.16	+0.36

those that are shorter or thinner with negative perturbations. The darker the color becomes, the greater the perturbation value becomes. Table I shows the perturbation values for each body part of Fig. 3. From the table, we find that the right and left sides of the whole body are longer and shorter, respectively. This result suggests that the attack on the length breaks the left-right symmetry of the body shape and throws the robot off balance. On the other hand, the table indicates that all the thicknesses increase, i.e., the attack on the thickness makes the robot heavier and more difficult to move than the clean one.

Figure 3c shows the animations of the walking simulations for clean (top), length attack (middle), and thickness attack (bottom). We see that the length-attacked robot (middle) loses its balance and falls. This result comes from the left-right asymmetry of the body, as shown in Fig. 3 and Table I. We also see that the thickness-attacked robot (bottom) falls. As mentioned above, the thickness attack weighs down the robot; thus, it becomes difficult for the robot to move the legs for stable walking.

Figure 4 shows the *average* of the 1000 average cumulative rewards in Eq. (12) for Walker2d-v2. In Fig. 4, the blue and orange bars show the average rewards of the attacks on the length and thickness, respectively. The results demonstrate that the average rewards decrease by attacking the body shape with strength $\epsilon \geq 0.05$, e.g., the length perturbation with $\epsilon = 0.05$ reduces the reward by 82% to the baseline

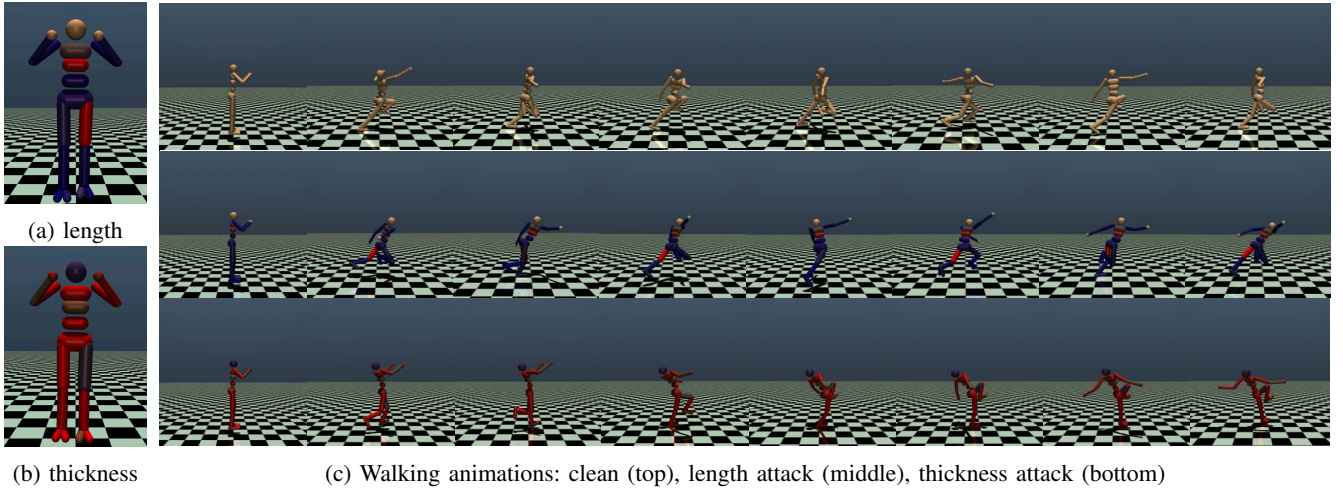


Fig. 7: Adversarial body shapes with length and thickness perturbations for Humanoid-v2.

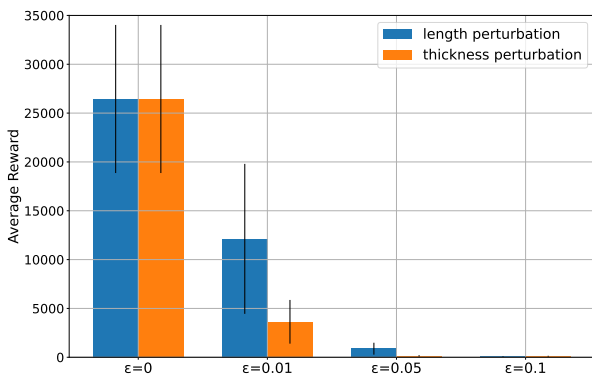


Fig. 8: Averages of the average cumulative rewards with attack strength $\epsilon = 0.0, 0.0.1, 0.05, 0.1$ for Humanoid-2d

($\epsilon = 0.0$). In particular, we find that Walker2d-v2 is more vulnerable to the attack on the length than the thickness of the body parts.

2) *Ant-v2*: Figure 5 visualizes the perturbations of the length and thickness with $\epsilon = 0.05$. Like Walker2d-v2 in Fig. 3, blue and red mean the positive and negative perturbations, respectively. Table II shows the perturbation values for each body part of Fig. 5. From the table, we find that the right front and left back parts are longer and the other two parts are shorter than the clean one. As shown in Fig. 5c (top), the clean Ant-v2 uses its right front and left back legs to move forward and uses the other legs to support its body. Hence, the adversarial perturbations in Table II cause a pitch oscillation of Ant-v2, as shown in Fig. 5c (middle). Unlike the length perturbation, the thickness perturbation has no significant effect on walking, as shown in Fig. 5c (bottom).

Figure 6 shows the average of the 1000 average cumulative rewards in Eq.(12) for Ant-v2. The results demonstrate that the length attack is successful with $\epsilon \geq 0.05$, whereas the thickness attack is not. For example, the length attack with $\epsilon = 0.05$ reduces the average reward by 60% to that of the clean one, and the thickness attack does not. These results indicate that Ant-v2 is vulnerable to the length attack and is robust to the thickness attack.

TABLE III: Adversarial body shape perturbation for thickness and length of Humanoid-v2

body part	length (%)	thickness (%)
head	-	+2.21
torso	+0.69	-3.11
upper waist	+3.71	-0.39
lower waist	-2.89	-3.78
pelvis	+3.36	-3.38
right thigh	+2.96	-4.91
right leg	+4.48	-4.09
right right foot	+4.65	-3.43
right left foot	+3.46	-3.85
left thigh	-4.54	+1.66
left leg	+3.84	-4.91
left right foot	+2.16	-0.93
left left foot	+4.41	-4.86
right upper arm	+3.69	-3.29
right lower arm	+3.35	+0.05
right hand	-	-1.86
left upper arm	+4.09	-3.09
left lower arm	+3.24	-2.9
left hand	-	-1.27

3) *Humanoid-v2*: Figure 7 visualizes the perturbations of the length and thickness with $\epsilon = 0.05$. Table III shows the perturbation values for each body part of Fig. 7. From the data in the table, we infer that the right leg parts—thigh, leg, right foot, and left foot—are longer and the left thigh is shorter than those of the clean one by attacking the lengths. Like that observed for Walker2d-v2, these adversarial length perturbations break the left-right symmetry of the body shape and throws the robot off balance, as shown in Fig. 7c (middle). On the other hand, Table III lists the thickness perturbations that make the head larger and the other parts thinner. As shown in Fig. 7c (bottom), the head of Humanoid-v2 is so heavy that it loses its balance and is pulled backward.

Figure 8 shows the average of the 1000 average cumulative rewards in Eq. (12) for Humanoid-v2. The results demonstrate that Humanoid-v2 is vulnerable to the adversarial attack on both the length and thickness, in relation to Walker2d-v2 and Ant-v2. Hence, both attacks can significantly reduce the average rewards with even $\epsilon \geq 0.01$, and the average rewards eventually become almost zero when $\epsilon = 0.1$.

V. CONCLUSION

We proposed an evolutionary computation method for searching adversarial body shapes of the legged robots. The vulnerability to small body changes can be a potentially significant risk, because they cause the robots to fall. Because deep reinforcement learning has been widely used in robotics, finding vulnerability is very important for the safety and robustness in robotics. This study demonstrated that the legged robots—Walker2d, Ant-v2, and Humanoid-v2—are vulnerable to the attacks on the body shape and can be forced to fall. Through the experiments, we revealed that the adversarial attacks perturb the length or thickness of the body parts such that the left-right symmetry is broken or the center of gravity is shifted. In future, we will develop a method to design robust body shapes against the adversarial attacks to improve the safety and robustness of legged robots.

REFERENCES

- [1] Eduardo F. Morales, Rafael Murrieta-Cid, Israel Becerra, and Marco A. Esquivel-Basaldua. A survey on deep learning and deep reinforcement learning in robotics with a tutorial on deep reinforcement learning. *Intell. Serv. Robot.*, 14(5):773–805, nov 2021.
- [2] Chaowei Xiao, Xinlei Pan, Warren He, Jian Peng, Mingjie Sun, Jinfeng Yi, Mingyan Liu, Bo Li, and Dawn Song. Characterizing attacks on deep reinforcement learning. *arXiv preprint arXiv:1907.09470*, 2019.
- [3] Inaam Ilahi, Muhammad Usama, Junaid Qadir, Muhammad Umar Janjua, Ala Al-Fuqaha, Dinh Thai Hoang, and Dusit Niyato. Challenges and countermeasures for adversarial attacks on deep reinforcement learning. *IEEE Transactions on Artificial Intelligence*, 3(2):90–109, 2022.
- [4] Rainer Storn and Kenneth Price. Differential evolution—a simple and efficient heuristic for global optimization over continuous spaces. *Journal of global optimization*, 11(4):341–359, 1997.
- [5] Greg Brockman, Vicki Cheung, Ludwig Pettersson, Jonas Schneider, John Schulman, Jie Tang, and Wojciech Zaremba. Openai gym, 2016.
- [6] Emanuel Todorov, Tom Erez, and Yuval Tassa. Mujoco: A physics engine for model-based control. In *2012 IEEE/RSJ International Conference on Intelligent Robots and Systems*, pages 5026–5033. IEEE, 2012.
- [7] David R Ha. Reinforcement learning for improving agent design. *Artificial Life*, 25:352–365, 2019.
- [8] Charles B. Schaff, David Yunis, Ayan Chakrabarti, and Matthew R. Walter. Jointly learning to construct and control agents using deep reinforcement learning. *2019 International Conference on Robotics and Automation (ICRA)*, pages 9798–9805, 2019.
- [9] Kevin Sebastian Luck, Heni Ben Amor, and Roberto Calandra. Data-efficient co-adaptation of morphology and behaviour with deep reinforcement learning. In *Proceedings of the Conference on Robot Learning*, pages 854–869, 2020.
- [10] Tingwu Wang, Yuhao Zhou, Sanja Fidler, and Jimmy Ba. Neural graph evolution: Automatic robot design. In *International Conference on Learning Representations*, 2019.
- [11] Tingwu Wang, Renjie Liao, Jimmy Ba, and Sanja Fidler. Nervenet: Learning structured policy with graph neural networks. In *International Conference on Learning Representations*, 2018.
- [12] Ruta Desai, Beichen Li, Ye Yuan, and Stelian Coros. Interactive co-design of form and function for legged robots using the adjoint method. *CoRR*, abs/1801.00385, 2018.
- [13] John Schulman, Filip Wolski, Prafulla Dhariwal, Alec Radford, and Oleg Klimov. Proximal policy optimization algorithms. *arXiv preprint arXiv:1707.06347*, 2017.